Supporting Information

Multi-Modulation for Self-Assemblies of Amphiphilic Rigid-Soft Compounds Through Alteration of Solution Polarity and Temperature

Xiaoying Li,[a],[b] Chun-Ting Poon,[b] Eugene Yau-Hin Hong,[b]   Hok-Lai Wong,[b]

Alan Kwun-Wa Chan,[b] Lixin Wu,*[a] and Vivian Wing-Wah Yam*[a],[b]

[a]State Key Laboratory of Supramolecular Structure and Materials and College of

Chemistry, Jilin University, Changchun 130012, P. R. China

[b]Institute of Molecular Functional Materials [Areas of Excellence Scheme,

University Grants Committee (Hong Kong)] and Department of Chemistry,

The University of Hong Kong, Pokfulam Road, Hong Kong, P. R. China

E-mail: wwyam@hku.hk

Crystallographic Data

Table S1 Crystal and structure determination data of compound **5**

|	
Empirical formula	$C_{74}H_{60}N_2O_{12} \cdot 2CH_2Cl_2$
Formula weight	1339.09
Temperature	296(2) K
Wavelength	0.71073 Å
Crystal system	Triclinic
Space group	$P\bar{1}$
Unit cell dimensions	a = 10.910(5) Å α = 103.07(2)°
	b = 13.241(8) Å β = 106.042(17)°
	c = 14.469(7) Å γ = 113.592(19)°
Volume	1701.1(16) Å^3
Z	4
Density (calculated)	1.307 mg m^{-3}
Absorption coefficient	0.238 mm^{-1}
F_{000}	698
Crystal size	0.47 mm × 0.15 mm × 0.11 mm
θ range for data collection	2.99 to 25.00°
Index ranges	$-12 \leq h \leq 11, -15 \leq k \leq 15, -17 \leq l \leq 17$
Reflections collected	13409
Independent reflections	5944 [R_{int} = 0.0596]
Completeness to θ = 25.242°	99.2 %
Absorption correction	Semi-empirical from equivalents
Max. and min. transmission	0.9743 and 0.8954
Refinement method	Full-matrix least-squares on F^2
Data / restraints / parameters	5944 / 0 / 448
Goodness-of-fit on F^2	1.055
Final R indices [$I > 2\sigma(I)$]	R_1 = 0.0731, wR_2 = 0.2118
R indices (all data)	R_1 = 0.1225, wR_2 = 0.2517
Large diff. peak and hole	0.629 and -0.731 eÅ^{-3}

Self-Assembly Studies
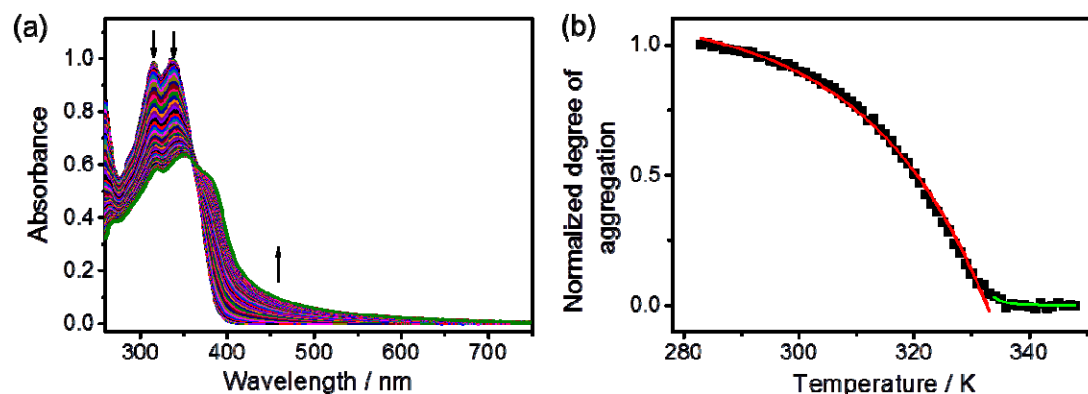
Figure S1. (a) UV-Vis absorption spectral traces on cooling a solution of **1** in 70 % DMSO−water mixture (1.2×10^{-5} M). (b) Plot of normalized degree of aggregation as a function of temperature, with curve fitting at the nucleation (green line) and the elongation (red line) regimes.
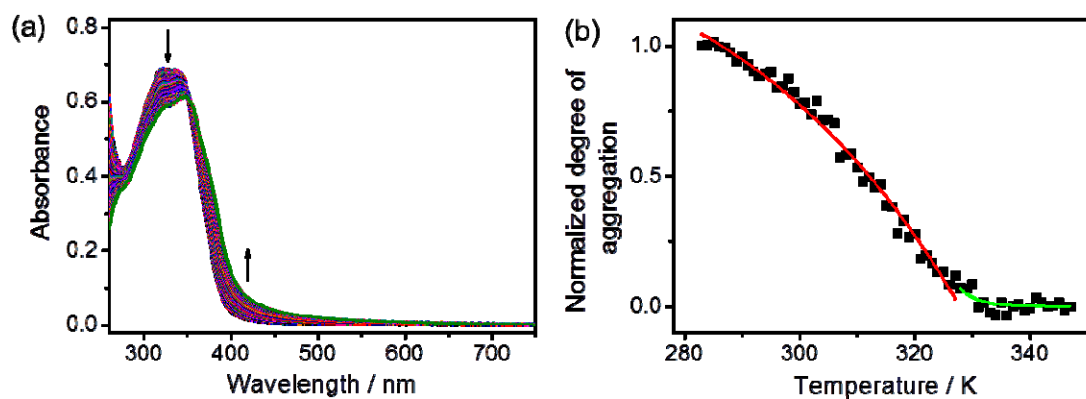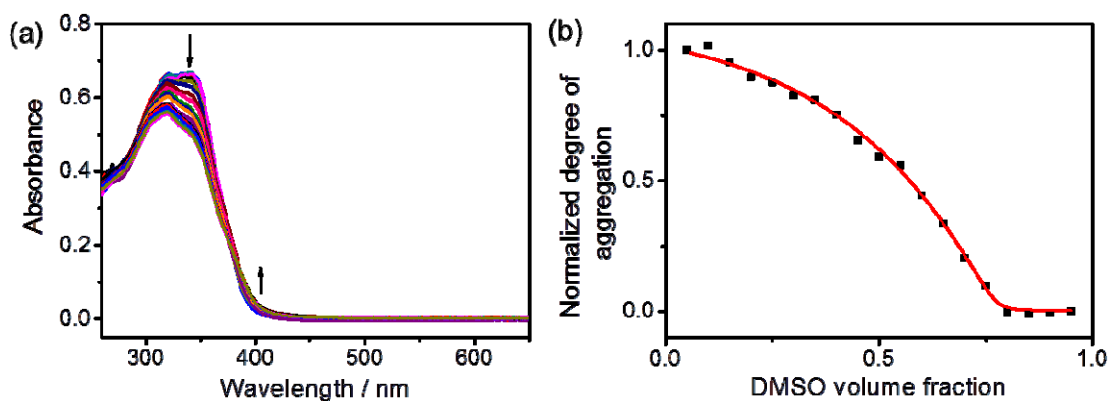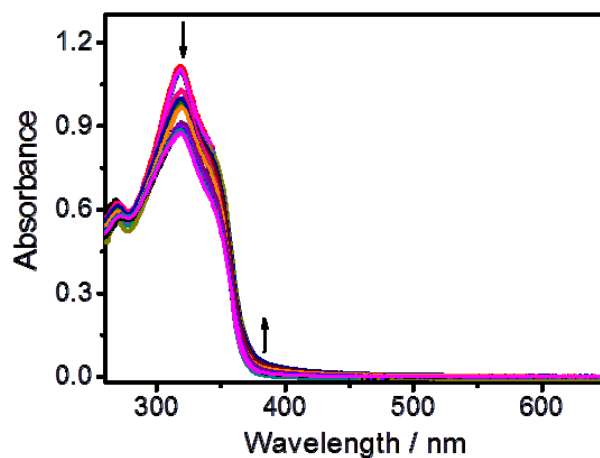

Figure S2. (a) UV-Vis absorption spectral traces on cooling a solution of **3** in 70 % DMSO−water mixture (1.2×10^{-5} M). (b) Plot of normalized degree of aggregation as a function of temperature, with curve fitting at the nucleation (green line) and the elongation (red line) regimes.
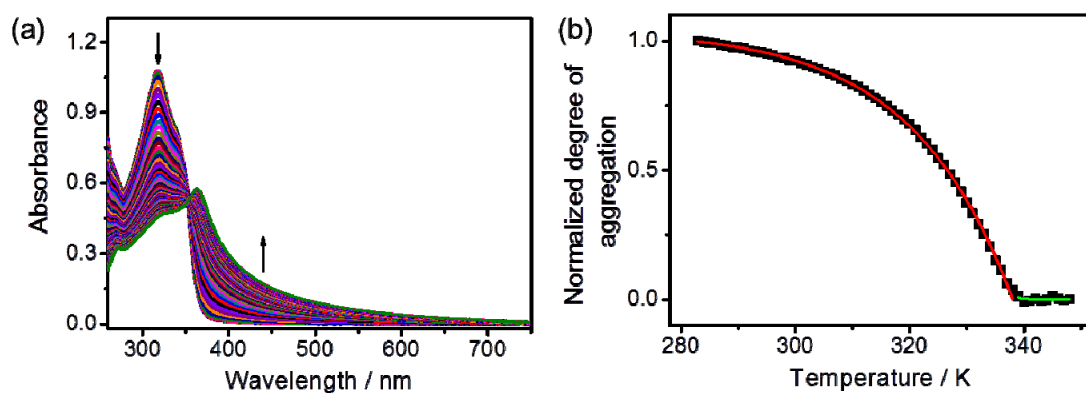
Figure S3. (a) UV-Vis absorption spectral traces on cooling a solution of **4** in 70 % DMSO–water mixture (1.6×10^{-5} M). (b) Plot of normalized degree of aggregation as a function of temperature, with curve fitting at the nucleation (green line) and the elongation (red line) regimes.
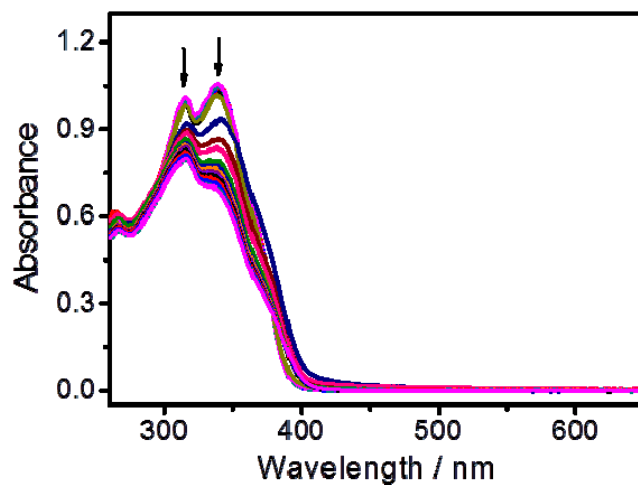
Figure S4. UV-Vis absorption spectral traces of **1** (1.2×10^{-5} M) upon increasing the water content in DMSO at 298 K.

Figure S5. (a) UV-Vis absorption spectral traces of **3** (1.2 × 10⁻⁵ M) upon increasing the water content in DMSO at 298 K. (b) Plot of normalized degree of aggregation as a function of DMSO volume fraction with curve fitting to the nucleation–elongation model.


Figure S6. UV-Vis absorption spectral traces of **4** (1.6 × 10⁻⁵ M) upon increasing the water content in DMSO at 298 K.
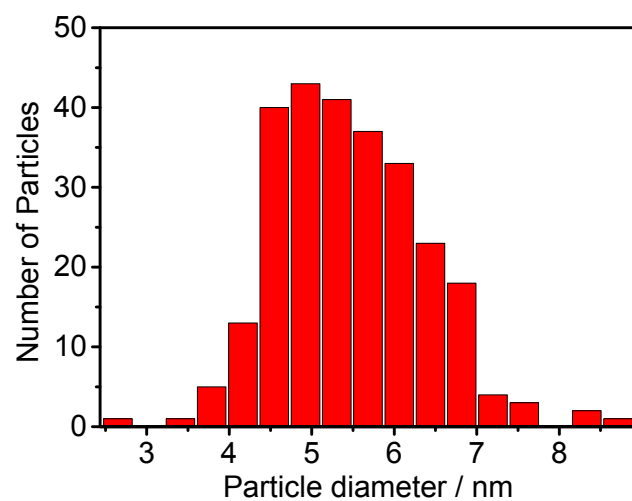
Figure S7. Statistical distribution of the particle sizes (total 265) taken from the TEM image in Figure 7a for compound **4** in aqueous solution (1.5×10^{-3} M) at room temperature.
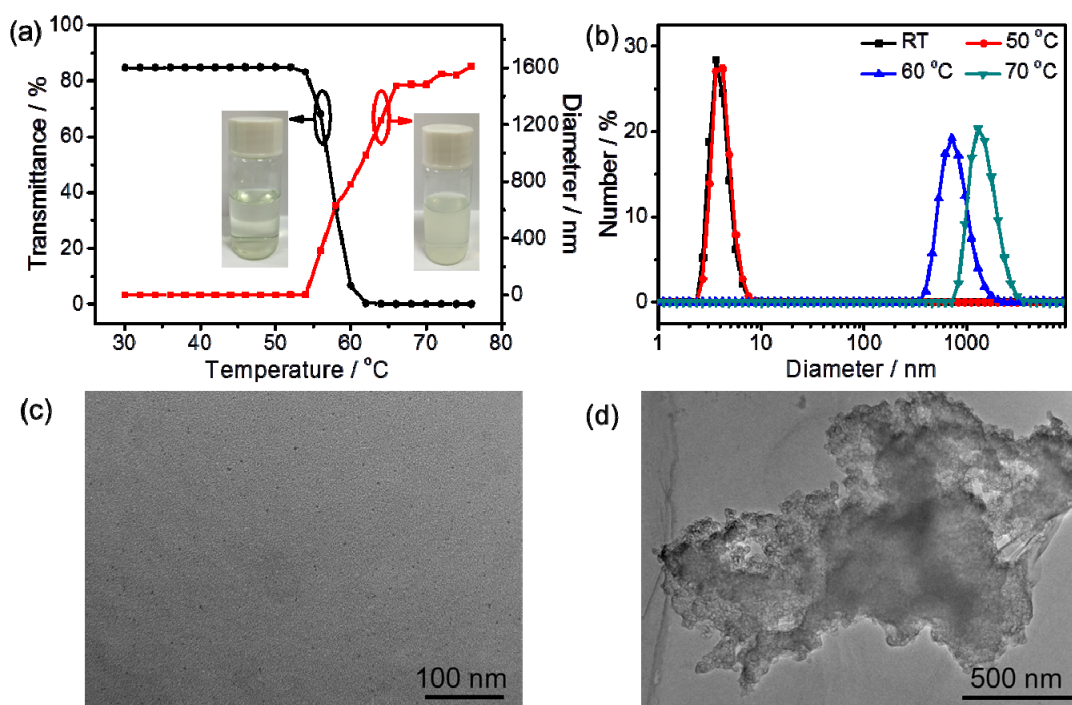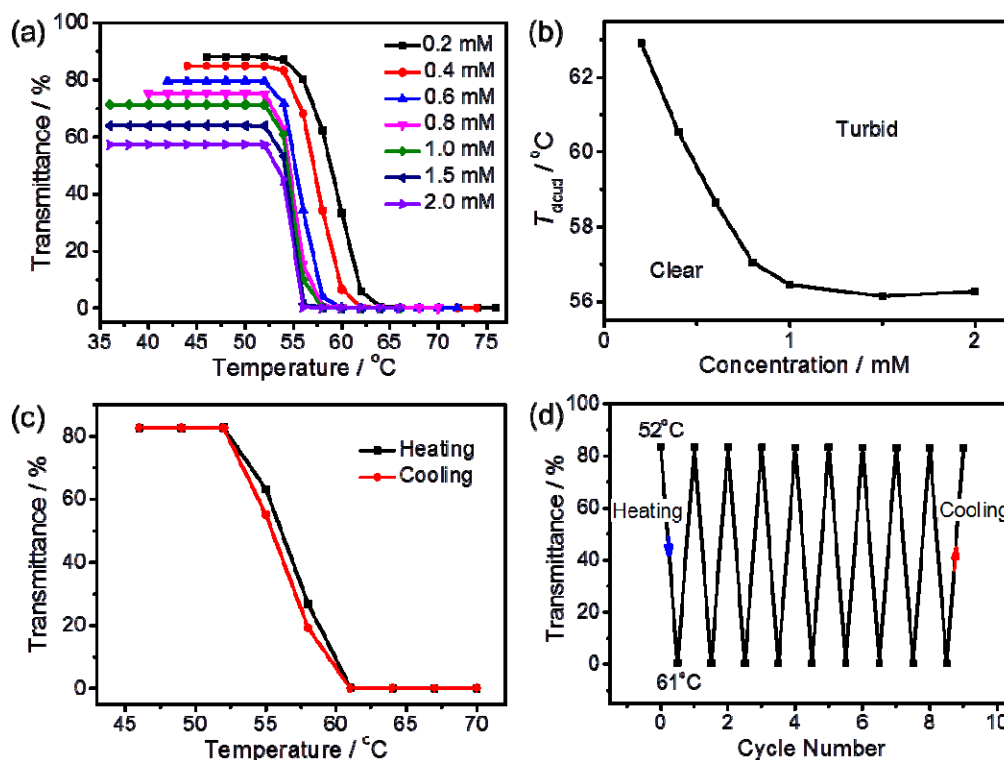
Figure S8. (a) Turbidity curves (measured at 550 nm) and the plot of hydrodynamic diameter obtained from DLS *via* heating of **3** in aqueous solution (4.0 × 10^{-4} M). Insets: Photographs of the aqueous solutions below and above cloud point temperature (T_{cloud}). (b) Size distributions of **3** in aqueous solution (4.0 × 10^{-4} M) for selected temperatures from DLS. (c) TEM images of the aggregates prepared from **3** in aqueous solution (4.0 × 10^{-4} M) at room temperature. (d) TEM images of the aggregates prepared from **3** in aqueous solution (4.0 × 10^{-4} M) at 65 °C.
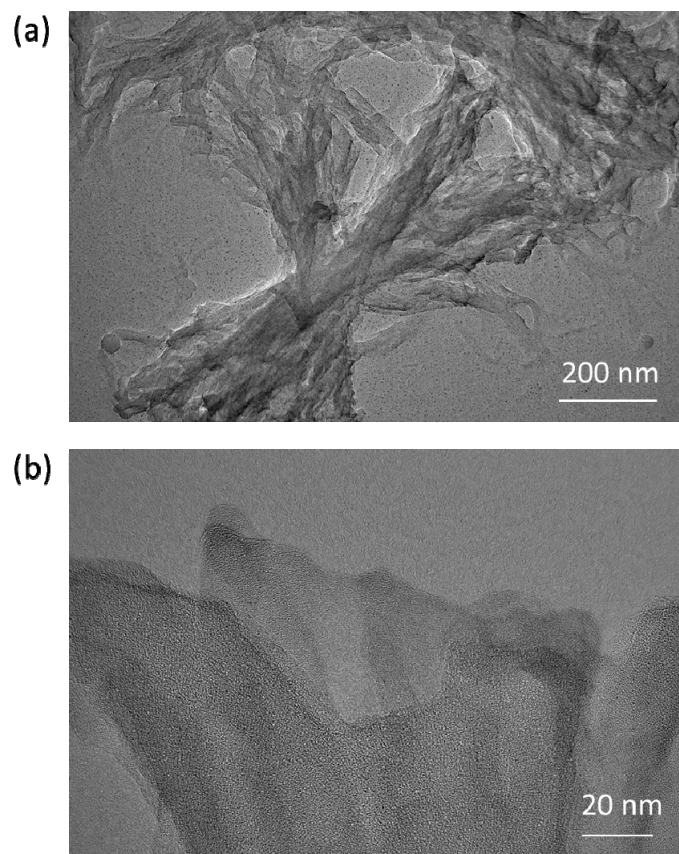
Figure S9. TEM images of compound **5** in the mixture of THF and ethanol with volume ratio of 1:1 at room temperature.

Figure S10. (a) Turbidity curves (measured at 550 nm) of **3** at different concentrations in aqueous solution. (b) Concentration dependence of the cloud point temperature (T_{cloud}) of **3** in aqueous solution. (c) Plots of transmittance at 550 nm of the aqueous solution of **3** (4×10^{-4} M) *via* a heating-cooling cycle. (d) Plots of transmittance at 550 nm of the aqueous solution of **3** (4×10^{-4} M) when cycling between $52\,^{\circ}C$ and $61\,^{\circ}C$.
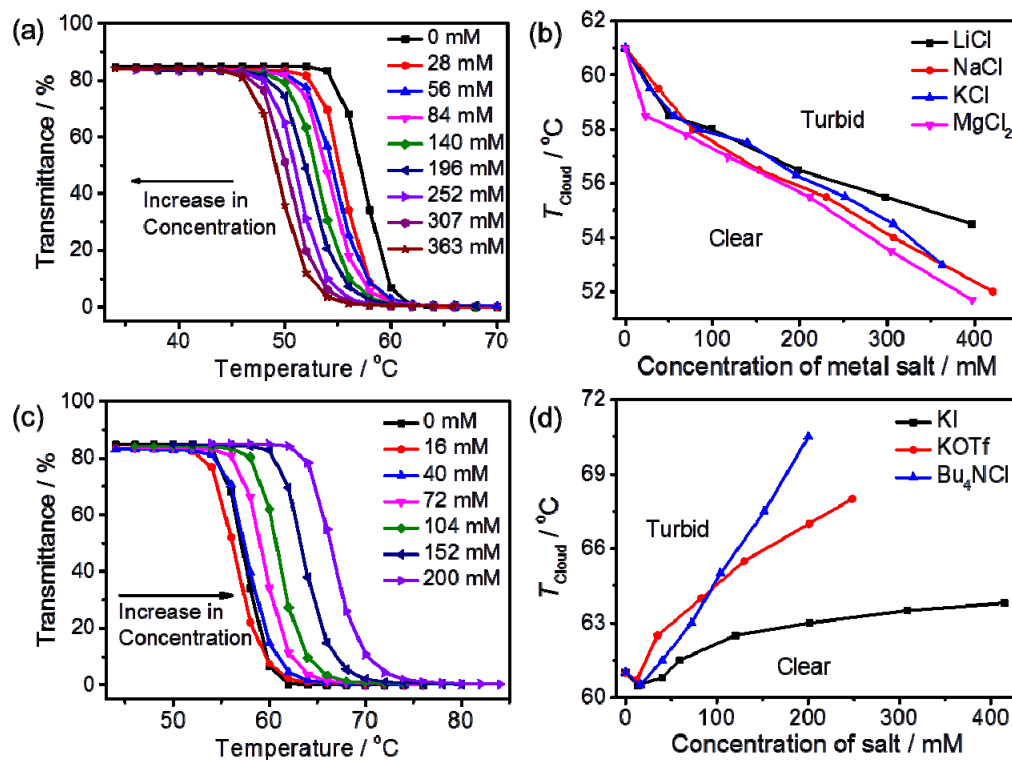
Figure S11. (a) Turbidity curves (measured at 550 nm) of **3** at different concentrations of K^+ in aqueous solution. (b) Concentration dependence of the cloud point temperature (T_{cloud}) of **3** in aqueous solution with different concentrations of Li^+, Na^+, K^+ and Mg^{2+}. (c) Turbidity curves (measured at 550 nm) of **3** at different concentrations of nBu$_4$NCl in aqueous solution. (d) Concentration dependence of the cloud point temperature (Tcloud) of **3** in aqueous solution with different concentrations of KI, KOTf and nBu$_4$NCl.

NMR Spectra
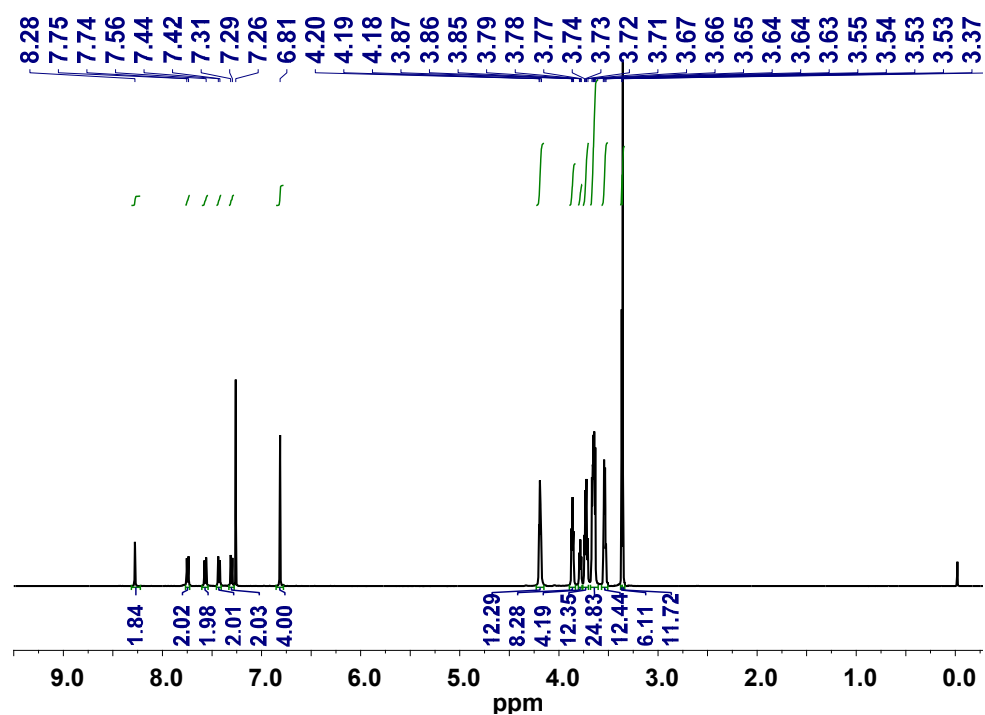
Figure S12. ^{1}H NMR spectrum of 9-(4-bromophenyl)-3,6-bis((3,4,5-tris(triethyleneglycol methyl ether)phenyl)ethynyl)-9*H*-carbazole in CDCl$_3$.
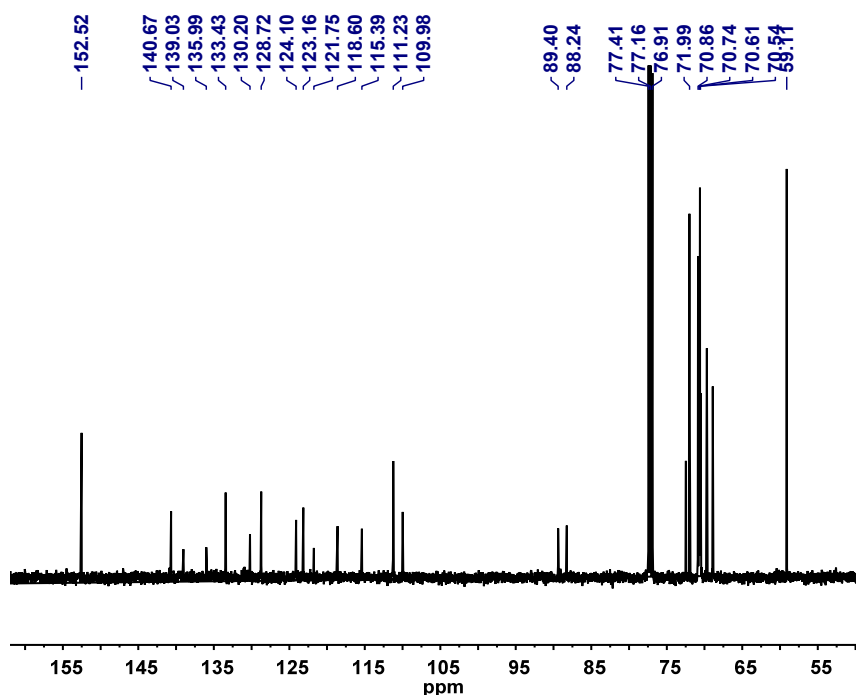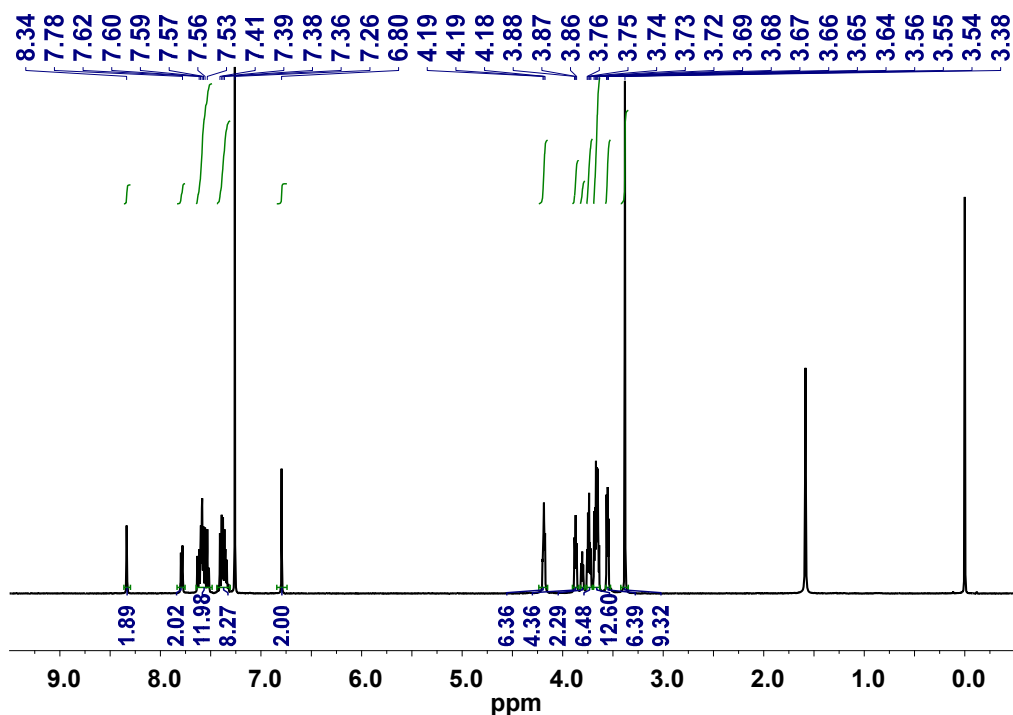

Figure S13. ^{13}C{^{1}H} NMR spectrum of 9-(4-bromophenyl)-3,6-bis((3,4,5-tris(triethyleneglycol methyl ether)phenyl)ethynyl)-9*H*-carbazole in CDCl$_3$.
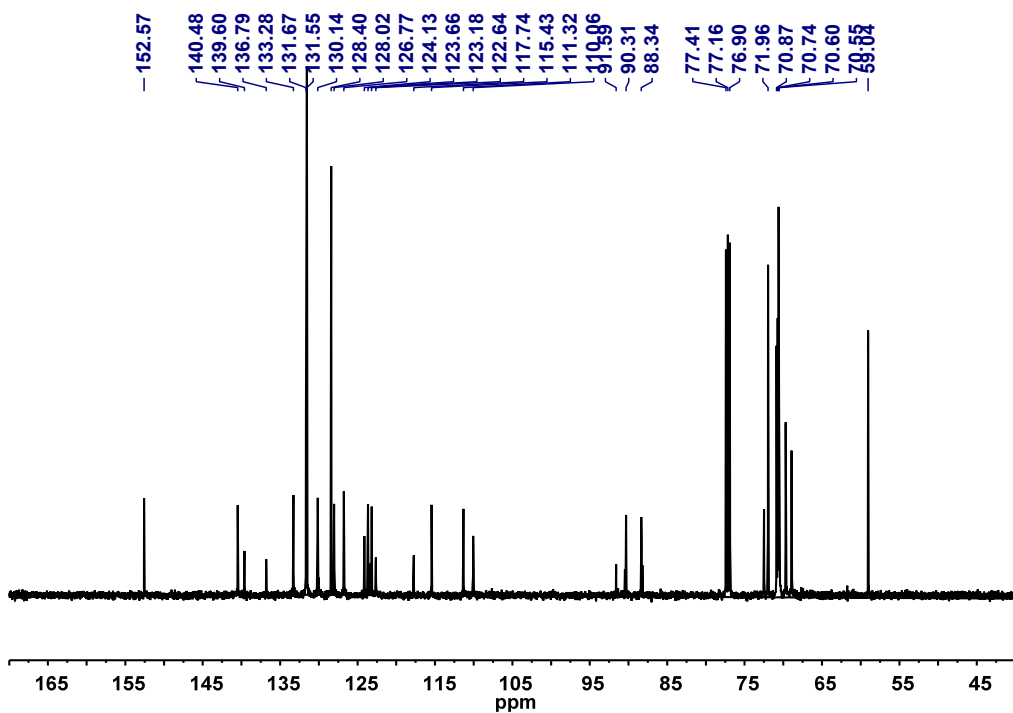
Figure S14. ^{1}H NMR spectrum of **1** in CDCl$_3$.

Figure S15. ^{13}C{^{1}H} NMR spectrum of **1** in CDCl$_3$.
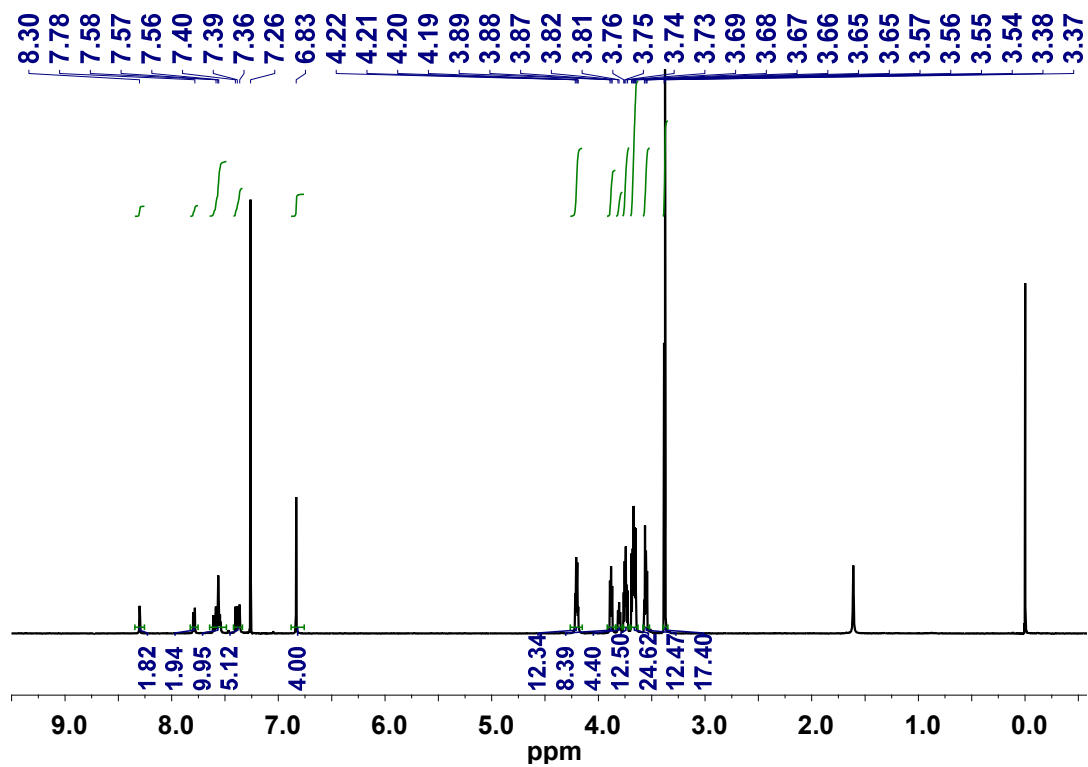
Figure S16. ^{1}H NMR spectrum of **2** in CDCl$_3$.
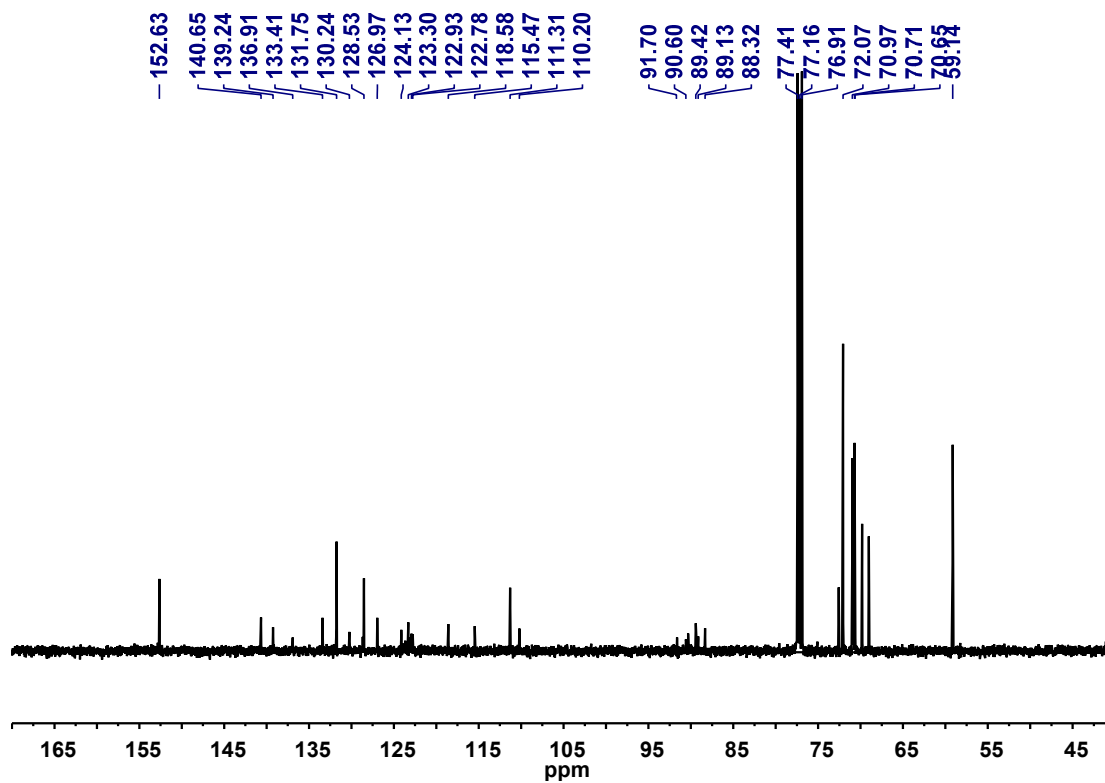
Figure S17. ^{13}C{^{1}H} NMR spectrum of **2** in CDCl$_3$.
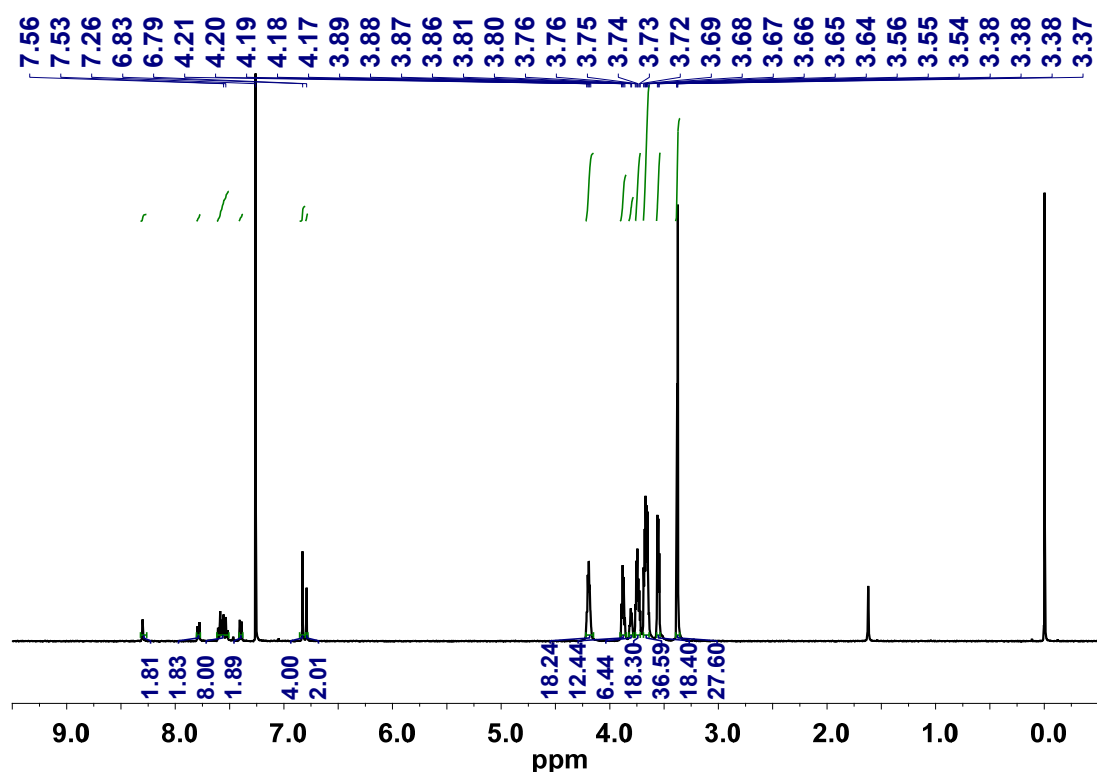
Figure S18. ^{1}H NMR spectrum of **3** in CDCl$_3$.
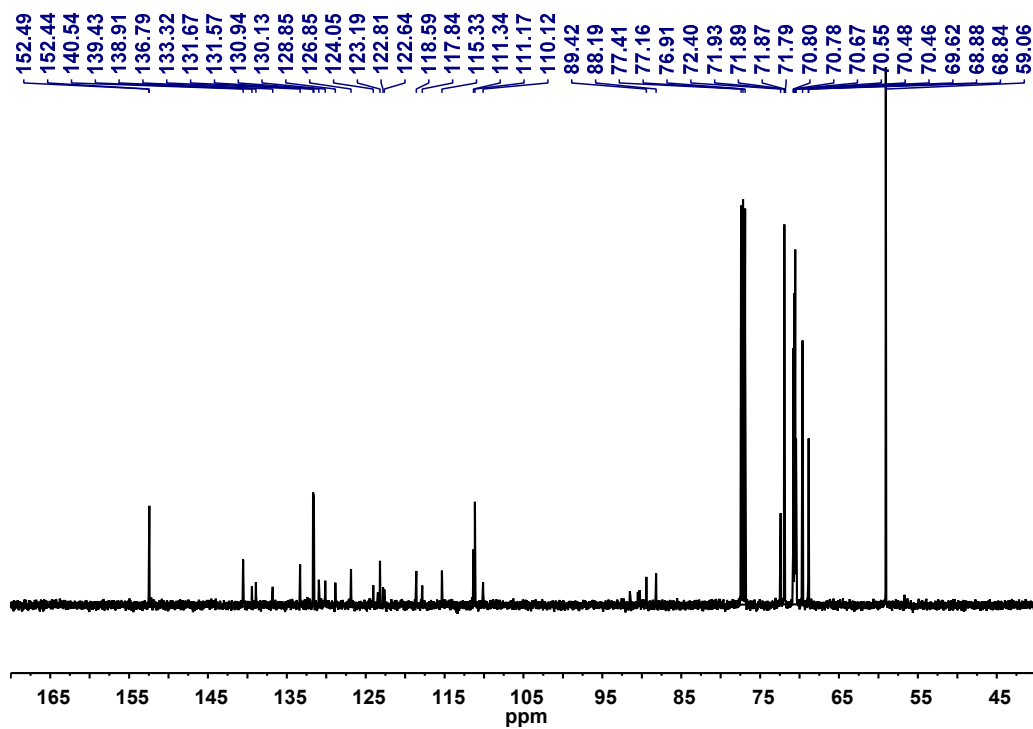
Figure S19. ^{13}C{^{1}H} NMR spectrum of **3** in CDCl$_3$.
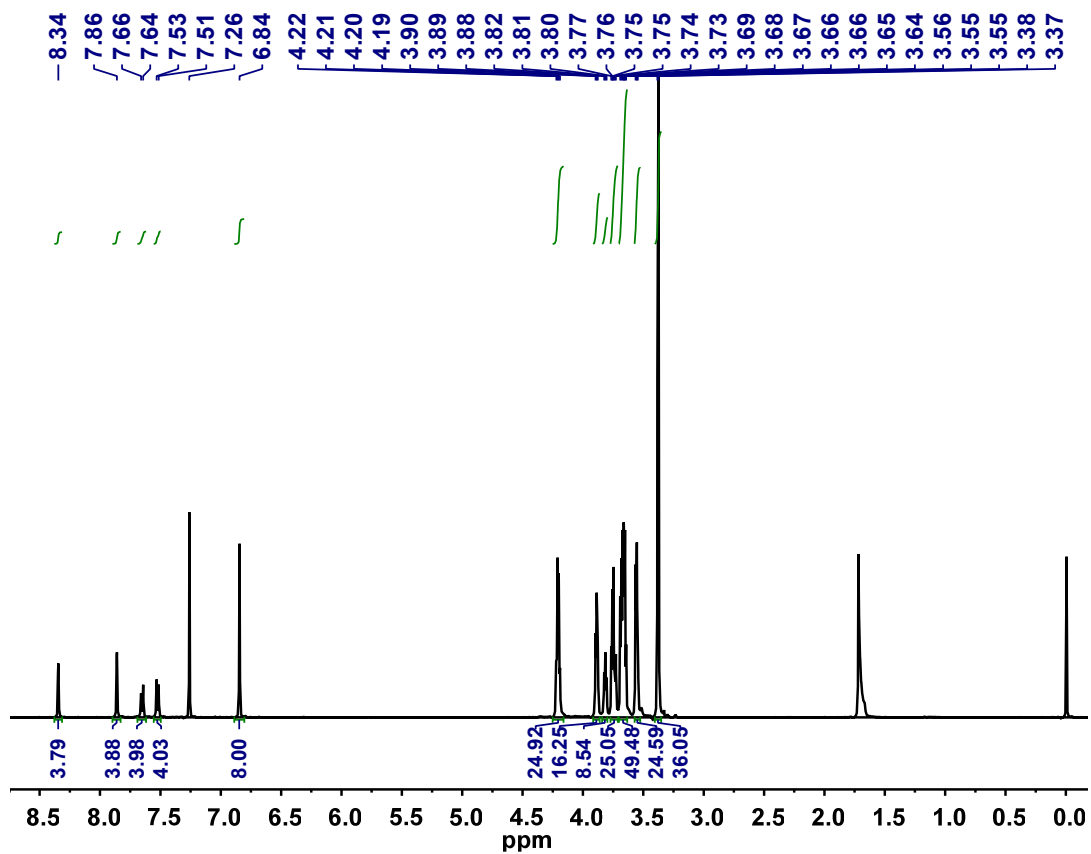
Figure S20. ^{1}H NMR spectrum of **4** in CDCl$_3$.
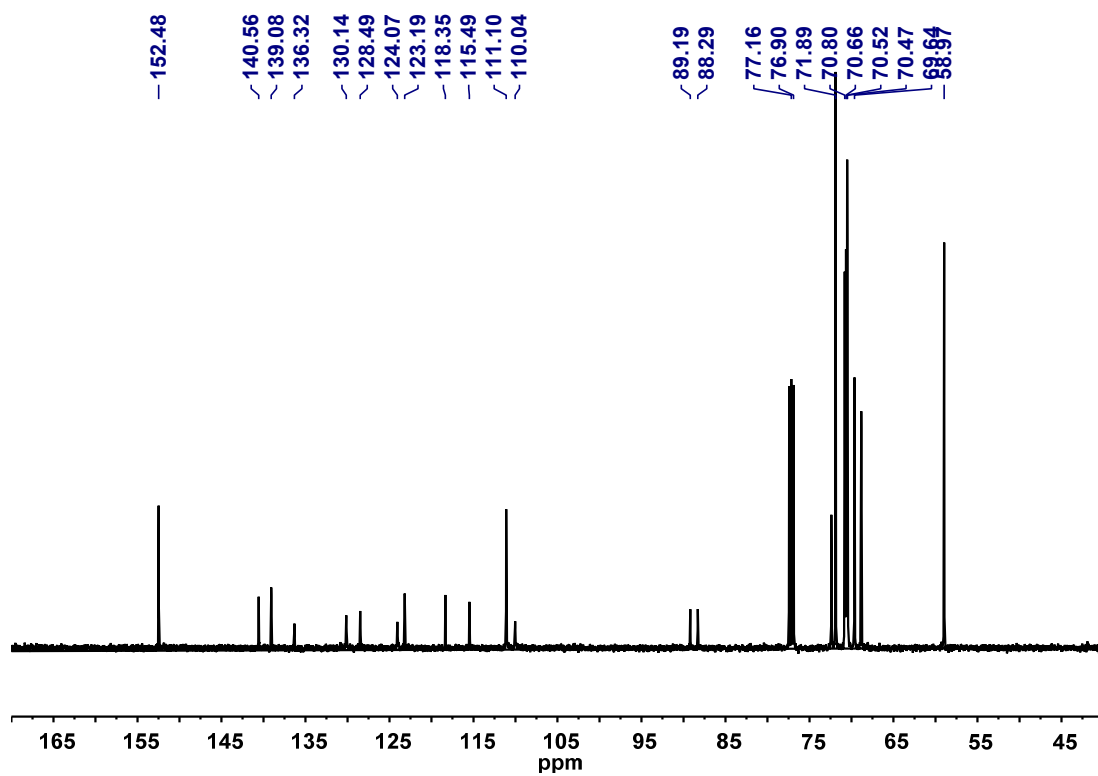
Figure S21. ^{13}C{^{1}H} NMR spectrum of **4** in CDCl$_3$.
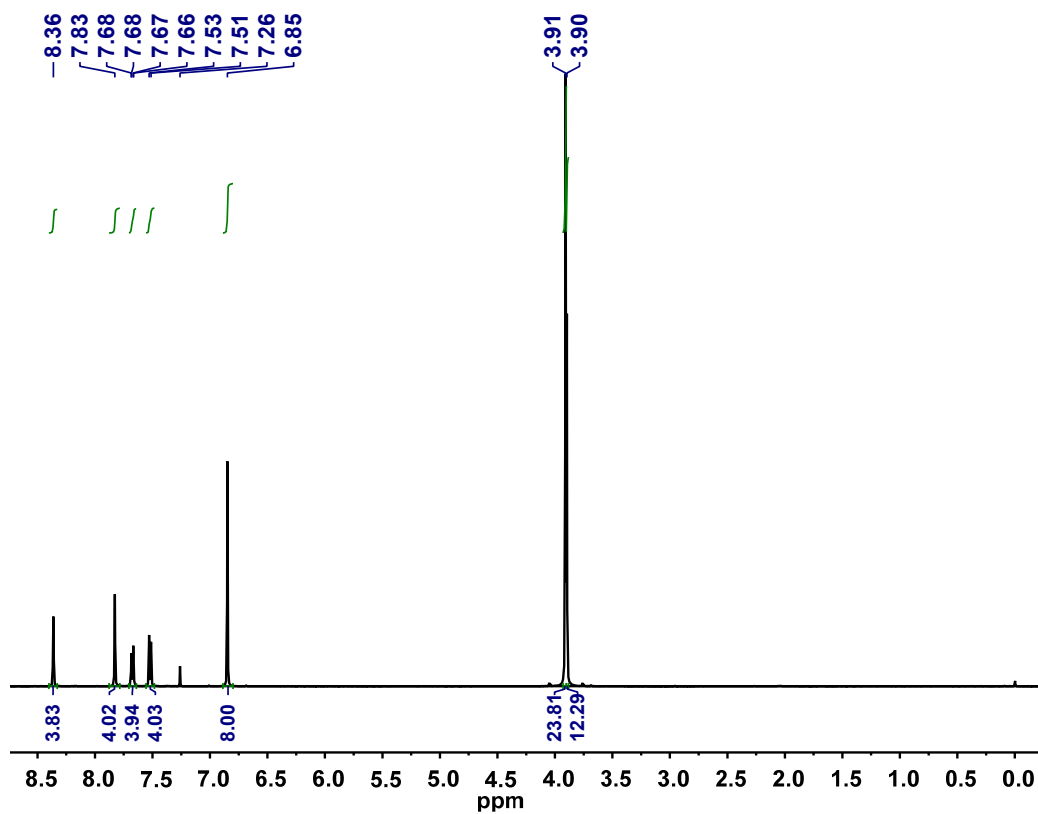
Figure S22. ^{1}H NMR spectrum of **5** in CDCl$_3$.
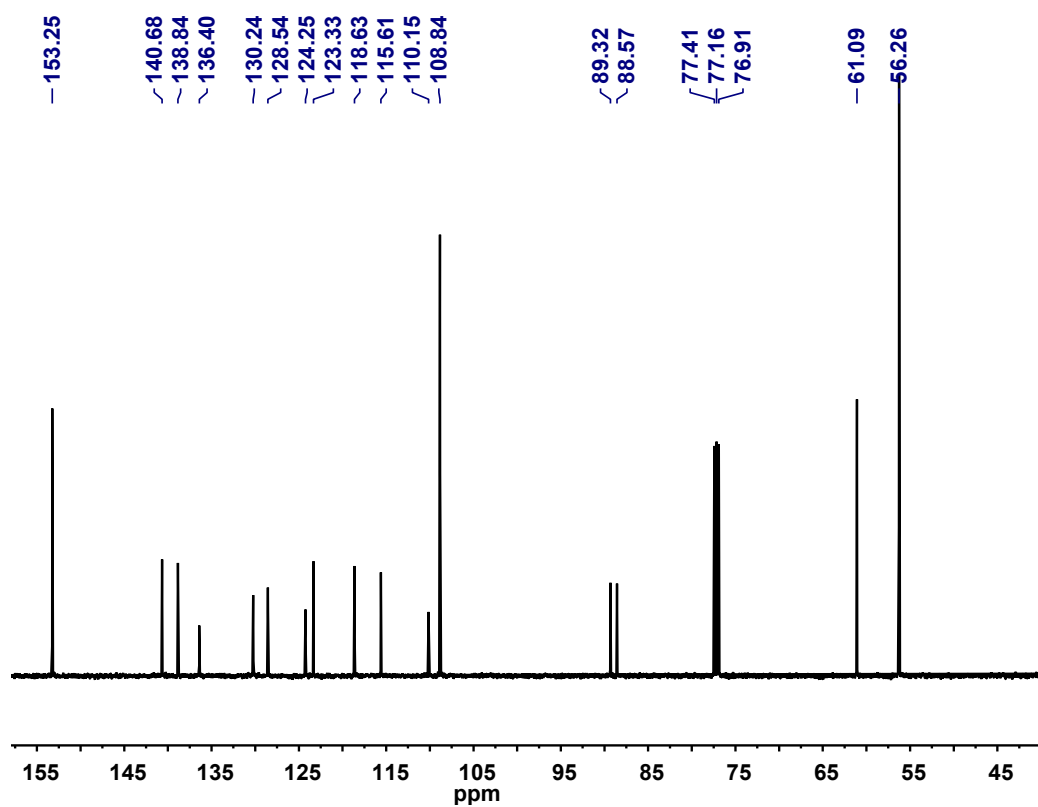
Figure S23. ^{13}C{^{1}H} NMR spectrum of **5** in CDCl$_3$.